Supplement of Atmos. Chem. Phys., 22, 10567–10587, 2022
https://doi.org/10.5194/acp-22-10567-2022-supplement

Atmospheric Chemistry and Physics
Open Access

Supplement of

Variations and sources of volatile organic compounds (VOCs) in urban region: insights from measurements on a tall tower

Xiao-Bing Li et al.

Correspondence to: Bin Yuan (byuan@jnu.edu.cn)

Table S1. Average mixing ratio, limits of detection (LOD), and instrument sensitivity for the VOC species reported in this study.

m/z	Chemical Formula	Suggested Compounds[@]	Average mixing ratio (pptv)	LOD** (pptv)	Sensitivity (cps/ppb)
26.015	C_2H_2	alkyl frag	8.3	4.2	686.8
27.023	C_2H_3	acetylene, alkyl frag	7.4	4.9	705.3
28.031	C_2H_4	alkyl frag	6.0	5.2	723.5
31.018	$CH_2OH^{\#\#}$	Formaldehyde*	4532.4	12.9	298.1
33.033	$CH_4OH^{\#\#}$	Methanol*	8680.0	22.4	466.6
41.039	$C_3H_5^{\#\#}$	aromatic frag, propyne, methylcyclopentane frag, MBO frag	112.1	9.6	937.1
42.034	$C_2H_3NH^{\#\#}$	Acetonitrile*	191.8	2.6	1261.6
42.046	C_3H_6	cyclopentane frag	5.5	1.7	952.0
43.018	C_2H_2OH	oxygenate frag, ketene	755.6	7.8	1357.3
43.054	C_3H_6H	alkyl frag, propene, propanol	413.1	6.3	966.8
44.049	$C_2H_5NH^{\#\#}$	etheneamine	3.5	2.4	1230.1
45.033	$C_2H_4OH^{\#\#}$	Acetaldehyde*	2535.8	10.0	1356.3
46.029	$CH_3NOH^{\#\#}$	formamide[#]	24.4	3.6	1218.1
47.013	$CH_2O_2H^{\#\#}$	formic acid[#]	749.5	40.8	331.2
47.049	$C_2H_6OH^{\#\#}$	Ethanol*	15824.2	113.7	197.7
48.044	CH_5NOH	hydroxy methyl amine	1.3	0.6	2179.2
49.028	CH_4O_2H	methane diol, formaldehyde water cluster	6.7	2.1	1435.3
49.011	CH_4SH	methane thiol	4.3	1.2	1381.9
51.044	CH_6O_2H	methanol water cluster	1792.2	7.1	1462.6
51.023	C_4H_2H	aromatic frag, butadiyne	5.0	3.4	1077.6
51.995	ClH_2NH	monochloramine	1.9	1.0	1706.6
53.039	C_4H_4H	Isoprene frag, alkyl frag, butenyne	4.4	2.1	1103.6

54.034	$C_3H_3NH^{\#\#}$	acrylonitrile	4.6	0.5	2758.4
57.033	$C_3H_4OH^{\#\#}$	Acrolein*	192.2	13.2	1691.7
57.070	C_4H_9	butenes, alkyl frag, butanol	798.2	1.0	1204.8
58.029	$C_2H_3NOH^{\#\#}$	methyl isocyanate, hydroxy acetonitrile	6.0	0.8	2103.9
59.049	$C_3H_6OH^{\#\#}$	Acetone*	4386.8	6.7	1755.1
60.044	$C_2H_5NOH^{\#\#}$	acetamide#	42.1	2.9	1693.6
61.028	$C_2H_4O_2H^{\#\#}$	Acetic acid#	4792.9	34.8	661.5
62.024	$CH_3NO_2H^{\#\#}$	nitromethane	10.2	1.3	2520.9
63.044	$C_2H_6O_2H^{\#\#}$	ethane diols, acetaldehyde water cluster, ethyl hydroperoxide, ethylene glycol	366.1	5.1	1522.0
65.023	CH_4O_3H	formic acid water cluster	57.7	3.5	1804.9
65.060	$C_2H_8O_2H$	ethanol water cluster	1246.2	34.8	1605.2
67.039	CH_7O_3	methane diol water cluster	2.1	0.7	1821.4
67.054	$C_5H_6H^{\#\#}$	cyclopentadiene, monoterpene frag	11.3	2.1	1267.6
68.049	$C_4H_5NH^{\#\#}$	pyrrole#	4.3	1.3	1205.7
68.062	C_5H_8	alkyl frag	4.7	1.4	1278.2
69.055	CH_8O_3H	methanol +2 water cluster	26.9	1.4	1836.9
69.033	$C_4H_4OH^{\#\#}$	Furan*	30.5	3.6	1194.0
69.070	$C_5H_8H^{\#\#}$	Isoprene*	293.7	4.5	1068.7
70.065	$C_4H_7NH^{\#\#}$	butane nitrile	11.6	1.0	2756.5
71.049	$C_4H_6OH^{\#\#}$	Methy Vinyl Ketone*, MACR	316.5	3.7	1919.5
71.086	$C_5H_{10}H$	pentenes, alkyl frag, C2 and C3 cyclhexanes	271.6	3.9	1308.1
72.044	C_3H_5NOH	ethyl isocyanate, Methoxyacetonitrile, acrylamide	4.8	0.9	3113.7
72.057	C_4H_8O	C4 carbonyl	11.8	1.3	1552.1

73.028	$C_3H_4O_2H^{\#\#}$	O_2+ product methyl glyoxal, acrylic acid	57.7	2.4	1713.7
73.065	$C_4H_8OH^{\#\#}$	2-Butanone/Methyl Ethyl Ketone*	1183.9	9.4	1938.2
73.101	$C_5H_{12}H$	pentanes (esp isopentane)	13.3	1.5	1329.2
74.060	$C_3H_7NOH^{\#\#}$	C3 amides	177.2	2.1	2708.0
75.044	$C_3H_6O_2H^{\#\#}$	Hydroxyacetone*, propionic acid, methyl acetate, ethyl formate	2288.1	14.6	1234.8
75.080	$C_4H_{10}OH$	butanols, monoterpene oxidation product	23.4	2.0	1569.0
76.039	$C_2H_5NO_2H^{\#\#}$	nitroethane	7.4	1.4	2439.2
77.023	$C_2H_4O_3H$	hydroxy or peroxyacetic acid (PAN indicator), glycolic acid	148.7	2.9	1972.0
77.060	$C_3H_8O_2H^{\#\#}$	acetone water cluster, C3 hydroperoxide, propane diols	200.4	3.0	1678.6
77.039	C_6H_5	aromatic frag	3.7	1.5	1367.5
78.046	C_6H_6	benzene charge transfer	8.8	1.2	1376.8
79.039	$C_2H_6O_3H$	acetic acid water cluster	277.2	5.8	1901.2
79.075	$C_3H_{10}O_2H$	propanol water cluster	24.6	1.1	1688.0
79.054	$C_6H_6H^{\#\#}$	Benzene*	384.7	3.4	1235.1
80.034	CH_5NO_3H	trihydroxy methyl amine	10.0	2.1	1394.9
80.990	C_2H_2FClH	chlorofluoroethene	23.4	1.0	1403.8
81.055	$C_2H_8O_3H$	ethane diol water cluster	12.1	1.7	1911.7
81.033	$C_5H_4OH^{\#\#}$	cyclopentadiene ketone	4.5	2.1	2483.4

81.070	C_6H_8H	monoterpene frag, decahydronapht halene frag	97.6	2.7	1403.9
83.013	$C_4H_2O_2H$	C4 2-oxy 4-DBE	5.0	1.3	1752.0
83.049	$C_5H_6OH^{\#\#}$	methyl furan, cyclopentenone, pent-2-ynal	36.8	2.5	1379.5
83.086	$C_6H_{10}H^{\#\#}$	hexadienes, methylcyclopent ane, cyclohexene, alkene or cycloalkane frag, hexenol and hexanal indicator	185.3	3.4	1421.4
84.081	$C_5H_9NH^{\#\#}$	C5 nitrile	4.4	0.9	2998.6
84.938	CrO_2H	chromium (stainless steel)	7.0	1.4	1709.9
85.028	$C_4H_4O_2H^{\#\#}$	furanone, hydroxy furan	24.6	3.9	1889.3
85.065	$C_5H_8OH^{\#\#}$	C5 ketones, cyclopentanone, 2ethylacrolein, dihydromethylfu ran, dihydropyran, MBO NO+	52.0	2.4	2352.7
85.101	$C_6H_{12}H^{\#\#}$	methylcyclopent ane, pentenes, cyclohexane frag, butadione,	140.0	2.9	1438.4
87.044	$C_4H_6O_2H^{\#\#}$	methyl acrylate, vinyl acetate, dihydrodioxin, butyrolactone	210.3	4.5	1717.0
87.080	$C_5H_{10}OH^{\#\#}$	2-Pentanone* acetone NO+	102.7	2.7	1997.9
88.039	$C_3H_6NO_2$	product, nitropropenes, oxazolidone	20.0	1.2	2791.9
88.076	C_4H_9NOH	C2 acetamides,	54.1	1.4	2791.9

89.023	$C_3H_4O_3H^{\#\#}$	C4 amides, morpholine oxo propanoic (pyruvic) acid, acetic-formic acid anhydride, APAN indicator	5.7	3.5	1946.3
89.060	$C_4H_8O_2H^{\#\#}$	ethyl acetate, butryic acid, hydroxy butanone, acetoin	2773.7	6.6	1059.3
89.096	$C_5H_{12}OH^{\#\#}$	pentanols	14.5	1.0	1679.4
91.039	$C_3H_6O_3H^{\#\#}$	hydroxy or peroxypropanoic acid, PPN indicator	315.8	4.9	2030.7
91.075	$C_4H_{10}O_2H^{\#\#}$	butane diols, C4 carbonyl water cluster	60.3	1.5	2171.6
91.054	C_7H_6H	aromatic frag	155.1	4.3	1486.6
92.062	C_7H_8	toluene charge transfer	62.9	1.7	1494.2
93.055	$C_3H_8O_3H$	propanoic acid water cluster	104.8	6.6	1959.7
93.091	$C_4H_{12}O_2H$	C4 alcohol water cluster	67.8	1.2	1738.2
93.033	C_6H_4OH	ethyne furan	273.2	14.3	1663.4
93.070	$C_7H_8H_{\#\#}$	Toluene*	1483.6	1.2	1539.0
95.049	$C_6H_6OH_{\#\#}$	Phenol*	20.6	3.9	1513.1
95.086	$C_7H_{10}H_{\#\#}$	decahydronaphthalene frag, monoterpene frag	28.7	2.1	1516.6
96.961	$C_2H_2Cl_2H$	dichloroethene (uncertain ID)	25.0	1.3	1531.0
97.065	$C_6H_8OH^{\#\#}$	dimethyl or ethyl furan, hexadienal, methylcyclopentenone, cyclohexeneone	25.7	2.4	1465.8
97.101	$C_7H_{12}H^{\#\#}$	methylcyclohexane frag, urban	86.3	2.7	1531.0

		OA, monoterpene frag, methylcyclohexene			
98.073	$C_6H_{10}O$	C6 carbonyl +1DBE O_2+ product	4.2	1.2	1687.0
99.008	$C_4H_2O_3H$	C4 3-oxy 4DBE: maleic anhydride	17.1	3.2	2049.5
99.044	$C_5H_6O_2H^{\#\#}$	methyl furanone, methanol furan	32.4	3.7	2955.8
99.080	$C_6H_{10}OH^{\#\#}$	hexenones, methylcyclopentanone, cyclohexanone	209.9	2.1	2387.0
99.117	$C_7H_{14}H$	methylcyclohexane, dimethylcyclopentane, alkanes frag	25.1	1.8	1513.5
100.039	$C_4H_5NO_2H$	MVK NO^+ product	5.3	1.5	2669.9
100.076	C_5H_9NOH	C5 alkene amide, butyl isocyanate, C5 hydroxy nitrile	7.4	1.4	2839.8
101.023	$C_4H_4O_3H^{\#\#}$	C4 3-oxy 3DBE	26.9	4.3	2052.8
101.060	$C_5H_8O_2H^{\#\#}$	methyl methacrylate, pentanedione, propenyl ester	201.9	5.2	1675.8
101.096	$C_6H_{12}OH^{\#\#}$	acetic acid, acetylacetone,ethyl acrylate Methyl Isobutyl Ketone*	116.6	2.6	1995.6
102.019	$C_3H_3NO_3H$	oxazolidine dione	3.0	1.5	1565.3
102.055	$C_4H_8NO_2$	C4 ketones NO^+ product, nitro C4 alkenes	6.3	0.9	2770.7

102.091	$C_5H_{11}NOH$	C5 amides	6.9	0.9	2845.8
103.039	$C_4H_6O_3H^{\#\#}$	acetic anhydride, MPAN and CPAN indicator	34.7	3.2	2247.4
103.075	$C_5H_{10}O_2H^{\#\#}$	pentanoic acids, methyl butanonate,propyl acetate	105.4	2.2	1659.9
105.055	$C_4H_8O_3H$	hydroxy or peroxy butanoic acid (from PiBN or PnBN), various acetic acid ethoxy and methoxy esters	37.9	2.0	2058.0
105.091	$C_5H_{12}O_2H$	pentane diols, C5 carbonyl water cluster	12.8	1.5	1817.4
105.033	C_7H_4OH	C7 1-oxy 6-DBE	24.8	2.2	1741.1
105.070	$C_8H_8H^{\#\#}$	Styrene*	136.6	2.5	1875.6
106.078	C_8H_{10}	C8 aromatics charge transfer	56.6	1.0	1591.0
107.034	$C_3H_6O_4H$	C3 4-oxy 1-DBE	5.2	1.6	2084.1
107.070	$C_4H_{10}O_3H$	C4 acid water cluster	25.5	2.2	1990.2
107.107	$C_5H_{14}O_2H$	C5 alcohol water cluster	51.3	1.2	1787.4
107.049	$C_7H_6OH^{\#\#}$	benzaldehyde	107.8	1.9	2490.6
107.086	$C_8H_{10}H^{\#\#}$	C8 aromatics*	1478.3	3.3	1699.3
109.050	$C_3H_8O_4H$	C3 tetrols	9.1	1.9	2085.7
109.028	$C_6H_4O_2H^{\#\#}$	benzoquinone	9.1	1.7	1924.4
109.101	$C_8H_{12}H^{\#\#}$	terpene frag	19.8	1.9	1697.6
111.065	$C_3H_{10}O_4H$	propanoic acid +2 water cluster	29.8	3.9	2017.1
111.044	$C_6H_6O_2H^{\#\#}$	methyl furfural, benzene diol, frag#	247.3	21.2	695.1
111.080	$C_7H_{10}OH^{\#\#}$	C3 substituted furan, biogenic oxidation product, C7	2.9	1.1	1552.5

		cylcoalkenones			
111.117	$C_8H_{14}H^{\#\#}$	C2 and C3 cyclohexanes frag, biogenic frag, octadiene	79.8	2.7	1621.1
113.023	$C_5H_4O_3H^{\#\#}$	methylfurandione, biogenic ox product	47.5	3.9	2063.2
113.060	$C_6H_8O_2H^{\#\#}$	dimethylfuranone, methyloxopentanal, biogenic ox product,	34.8	3.1	2081.4
113.096	$C_7H_{12}OH^{\#\#}$	hydroxy methyl cyclohexanone ethyl cyclopentanone	34.2	1.7	2398.1
113.132	$C_8H_{16}H$	dimethylcyclohexanes, alkane frag	34.6	2.0	1632.6
114.055	$C_5H_7NO_2H$	C5 1-nitro, 2-oxy, 3-DBE, C5 ketones +1DBE	7.2	1.0	2696.5
115.039	$C_5H_6O_3H^{\#\#}$	NO^+ product C5 3-oxy 3DBE	33.4	3.8	2063.5
115.075	$C_6H_{10}O_2H^{\#\#}$	C6 diketone isomers, vinylethyl acetate	79.3	3.3	1846.7
115.112	$C_7H_{14}OH^{\#\#}$	heptanal, dimethylpetnaone, heptanone	40.4	1.3	2398.0
116.906	CCl_3	carbon tet O_2^+ product	70.6	3.7	1654.7
117.018	$C_4H_4O_4H$	fumaric acid	5.9	2.7	2088.3
117.055	$C_5H_8O_3H^{\#\#}$	C5 3-oxy 2-DBE isomers,hydroxy ethyl acrylate butyl ester	23.7	3.4	2063.5
117.091	$C_6H_{12}O_2H^{\#\#}$	acetic acid,diacetonealcohol,butyl acetate	236.2	2.0	1810.7

117.127	$C_7H_{16}OH^{\#\#}$	C7 saturated alcohols	5.4	1.0	1777.4
118.050	$C_4H_7NO_3H^{\#\#}$	butene nitrates	8.5	1.8	1659.8
119.034	$C_4H_6O_4H$	butane dioic acid	10.2	3.1	2088.1
119.107	$C_6H_{14}O_2H^{\#\#}$	C6 saturated diols, C6 carbonyl water cluster,butoxy ethanol	104.1	1.9	1826.1
119.089	$C_6H_{14}SH$	C6 thiols/sulfides	6.3	1.3	1780.2
120.093	C_9H_{12}	C9 aromatics charge transfer	7.1	0.8	1670.1
121.065	$C_8H_8OH^{\#\#}$	tolualdehyde, acetophenone, dihydrobenzofuran, vinylphenol, benzeneacetaldehyde	64.5	1.8	2395.6
121.101	$C_9H_{12}H^{\#\#}$	C9 aromatics*	231.8	2.7	1800.9
122.008	$C_2H_3NO_5H$	C2H3NO5H+	13.2	1.9	1680.3
123.044	$C_7H_6O_2H^{\#\#}$	salicyladehyde, benzodioxole, benzoic acid	17.8	2.5	2382.2
123.080	$C_8H_{10}OH^{\#\#}$	4-ethylphenol, dimethylphenol, methylanisole	4.1	1.1	1797.4
123.117	$C_9H_{14}H$	terpene frag, santene	18.7	1.8	1685.0
124.039	$C_6H_5NO_2H^{\#\#}$	nitrobenzene	2.8	1.1	3081.4
125.060	$C_7H_8O_2H^{\#\#}$	Guaiacol*	10.9	3.0	2670.7
125.132	$C_9H_{16}H$	trimethylcyclohexane frag	51.2	2.2	1694.6
127.075	$C_7H_{10}O_2H$	furanone	20.4	3.0	1878.7
127.112	$C_8H_{14}OH^{\#\#}$	cyclooctanone	30.6	1.7	2390.3
127.148	$C_9H_{18}H$	trimethylcyclohexane	12.1	1.7	1703.9
129.055	$C_6H_8O_3H^{\#\#}$	methyloxopentenoic acid, acetylmethyloxiranecarbaldehyde	20.9	3.0	2057.5
129.091	$C_7H_{12}O_2H^{\#\#}$	allyl ester	40.4	2.7	1846.4

		isobutyric acid,butyl acrylate			
129.127	$C_8H_{16}OH^{\#\#}$	octanal	39.8	1.8	2388.0
129.070	$C_{10}H_8H^{\#\#}$	naphthalene*	34.3	3.3	2284.9
131.034	$C_5H_6O_4H$	C5 diacid +1DBE	10.7	2.8	2080.8
131.070	$C_6H_{10}O_3H$	dimethylfuranone, methyloxopentanal water cluster	22.9	2.4	2055.6
131.107	$C_7H_{14}O_2H^{\#\#}$	C7 carboxylic acid	13.8	1.7	1708.3
133.086	$C_6H_{12}O_3H^{\#\#}$	C6 hydroxy or peroxy acid,ethoxyethyl acetate	58.2	1.1	2053.5
133.076	$C_8H_8N_2H$	Methylpyrrolo[2-a]pyrazine, 1-methylindazole, benzimidazole	4.5	0.8	2470.2
133.101	$C_{10}H_{12}H^{\#\#}$	methyl-tetrahydronaphthalene, butenyl benzene, 2-phenyl 2-butene, ethyl styrene, isopropenyltoluene	28.5	1.4	1730.2
134.109	$C_{10}H_{14}$	C10 aromatics charge transfer	3.0	0.7	1734.3
135.102	$C_6H_{14}O_3H$	C6 acid water cluster	51.6	2.3	2051.4
135.138	$C_7H_{18}O_2H$	C7 alcohol water cluster	5.8	1.0	1870.2
135.117	$C_{10}H_{14}H^{\#\#}$	C10 aromatics	153.3	1.7	1738.4
136.022	C_7H_5NSH	benzothiazole	9.0	2.2	1742.6
137.060	$C_8H_8O_2H^{\#\#}$	phenyl ester of acetic acid, methyl ester of benzoic acid, toluene aromatic acid	14.7	2.2	1867.3
137.132	$C_{10}H_{16}H^{\#\#}$	Monoterpene*	276.0	3.3	902.9

139.042	$C_4H_{10}O_3SH$	sulfolane water cluster	3.7	1.7	1754.2
139.039	$C_7H_6O_3H$	salicylic acid, biogenic ox product, PBzN indicator	5.9	1.4	2047.6
139.112	$C_9H_{14}OH$	nopinone, C5 substituted furan	38.3	1.5	2373.4
139.148	$C_{10}H_{18}H$	C10 1DBE hydride abstraction	24.8	1.8	1754.0
140.034	$C_6H_5NO_3H$	benzene nitrophenol, benzene nitrate[#]	15.4	5.4	1526.2
141.127	$C_9H_{16}OH$[##]	C9 carbonyl +1DBE, C9 alcohol +2DBE	15.7	1.3	2370.2
141.164	$C_{10}H_{20}H$	C10 1DBE, C10 alkanes hydride abstraction	9.6	1.6	1761.5
143.107	$C_8H_{14}O_2H$	C8 2-oxy 2DBE isomers	23.3	2.3	1914.4
143.143	$C_9H_{18}OH$[##]	nonanal	87.7	2.0	2367.0
145.122	$C_8H_{16}O_2H$[##]	C8 carboxylic acid	22.5	1.9	1714.5
149.117	$C_7H_{16}O_3H$	C7 acid water cluster	19.4	1.4	1989.5
149.132	$C_{11}H_{16}H$[##]	C11 aromatics	26.4	1.2	1789.1
151.112	$C_{10}H_{14}OH$	pinonaldehyde, C10 aromatic alcohols	13.8	1.4	2004.7
151.148	$C_{11}H_{18}H$	C11 3-DBE	14.4	1.5	1795.5
153.055	$C_8H_8O_3H$[##]	methyl salicylate, C8 aromatic hydroxyacid	10.6	1.5	2034.5
153.127	$C_{10}H_{16}OH$[##]	apinene oxide, camphor, C6 substituted furans	23.8	1.7	1959.9
153.164	$C_{11}H_{20}H$	C11 2-DBE	11.6	1.5	1801.6
155.143	$C_{10}H_{18}OH$[##]	linalool, borneol,terpilenol	14.5	1.8	1876.6

155.179	$C_{11}H_{22}H$	C11 1-DBE, C11 alkanes	8.2	1.4	1807.5
157.159	$C_{10}H_{20}OH^{\#\#}$	NO+ product Menthol-type monoterpenes, decanal	38.0	2.5	1871.0
161.081	$C_7H_{12}O_4H$	C7 di-acids	9.8	1.6	2047.7
161.154	$C_9H_{20}O_2H$	C9 saturated diols, C9 carbonyl water cluster	13.1	1.3	1945.0
161.132	$C_{12}H_{16}H^{\#\#}$	aromatic frag	3.5	0.8	1824.3
163.133	$C_8H_{18}O_3H^{\#\#}$	C8 acid water cluster	7.8	1.9	1981.7
163.148	$C_{12}H_{18}H^{\#\#}$	C12 aromatics	7.0	1.4	1829.4
165.164	$C_{12}H_{20}H$	C12 3-DBE	13.1	1.5	1834.4
167.179	$C_{12}H_{22}H$	C12 2-DBE	7.6	1.4	1839.2
169.122	$C_{10}H_{16}O_2H$	pinonaldehyde, apinene hydroperoxide	17.1	2.0	1955.8
169.195	$C_{12}H_{24}H$	C12 1-DBE, alkyl frag	10.1	1.7	1843.8
171.174	$C_{11}H_{22}OH$	C11 1-oxy 1-DBE	10.0	1.4	1907.1
178.071	$C_6H_{11}NO_5H$	C6 1-nitro 5-oxy 2-DBE	2.4	1.0	1863.3
179.179	$C_{13}H_{22}H$	C13 3-DBE	11.8	1.4	1864.9
C14H10 H+	$C_{14}H_{10}H$	Anthracene or phenanthrene H_3O^+	20.6	2.6	1888.7
181.195	$C_{13}H_{24}H$	C13 2-DBE	6.4	1.4	1868.6
183.211	$C_{13}H_{26}H$		6.9	1.5	1872.2
185.190	$C_{12}H_{25}O$	Dodecanal	8.8	1.6	1910.1
191.179	$C_{14}H_{22}H$		8.2	2.9	1885.4
193.195	$C_{14}H_{24}H$		11.4	1.5	1888.4
195.174	$C_{13}H_{22}OH$	Solanone	2.4	1.1	1919.0
195.211	$C_{14}H_{26}H$		6.6	1.4	1891.2
197.226	$C_{14}H_{28}H$		7.3	1.6	1893.9
199.169	$C_{12}H_{22}O_2H$	Menthyl acetate	15.4	1.6	1965.3
203.179	$C_{15}H_{22}H$		5.0	1.2	1901.7
205.195	$C_{15}H_{24}H$		23.4	1.7	1904.0
207.211	$C_{15}H_{26}H$		9.8	1.3	1906.2
209.226	$C_{15}H_{28}H$	Drimane	5.8	1.3	1908.3
211.242	$C_{15}H_{30}H$		6.1	1.5	1910.3

215.179	$C_{16}H_{22}H$		4.7	1.4	1914.4
219.211	$C_{16}H_{26}H$	Perhydropyrene	6.9	1.6	1917.8
221.226	$C_{16}H_{28}H$		6.4	1.2	1919.4
223.064	$C_6H_{18}O_3Si_3H$	D3 Siloxane*	70.1	7.9	1074.9
297.082	$C_8H_{24}O_4Si_4H^{\#\#}$	D4 Siloxane*	41.5	6.8	872.1
299.062	$C_7H_{23}O_5Si_4$	D5 Siloxane frag	25.7	2.8	1948.9
371.101	$C_{10}H_{30}O_5Si_5H^{\#\#}$	D5 Siloxane*	15.1	6.7	709.5

* The VOC species are calibrated using the gas standard.

The VOC species are calibrated using the Liquid Calibration Unit (LCU).

** LOD of VOC species was derived at time resolutions of 10 s.

Reaction rate constants of the 105 species with OH radicals (Wu et al., 2020) were used in this study.

@ Suggested compounds of ion signals were determined according to the results in (Wu et al., 2020; Gkatzelis et al., 2021).

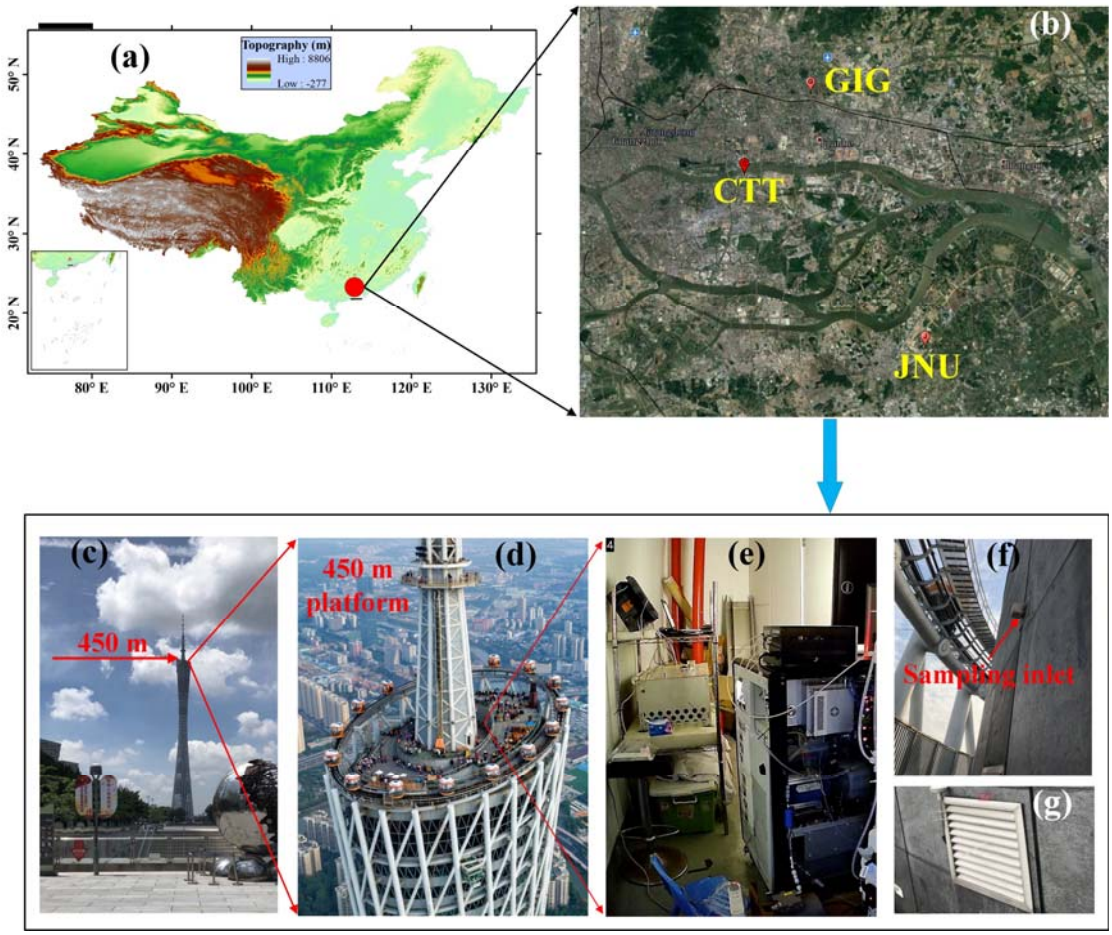

Figure S1. (a) Geographical location of the CTT site in China. (b) Geographical locations of the CTT, GIG, and JNU sites in Guangzhou. (c) Picture showing the CTT and the location of the 450 m Look Out platform. (d) Picture showing the 450 m Look Out platform. (e) Picture showing the instruments deployed in the observation room. (f) Picture showing the sampling inlet for instruments at the 450 m Look Out platform. (g) Picture showing the window of the observation room. Note that the map in panel (b) is extracted from © Google Maps by the authors; The picture in panel (d) is obtained from the website: https://720yun.com/t/ff8jusyvrk2?scene_id=23557335.

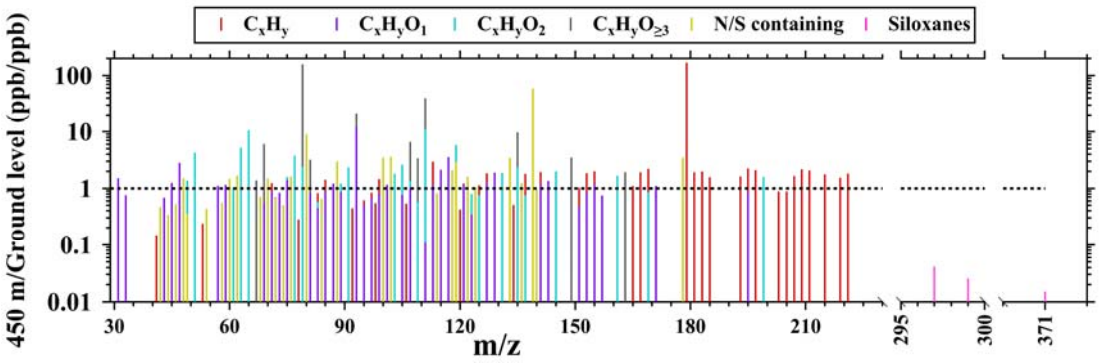

Figure S2. Average ratios of concentrations of various VOCs species measured at 450 m during the CTT campaign to those measured at ground level during the GIG campaign as a function of m/z.

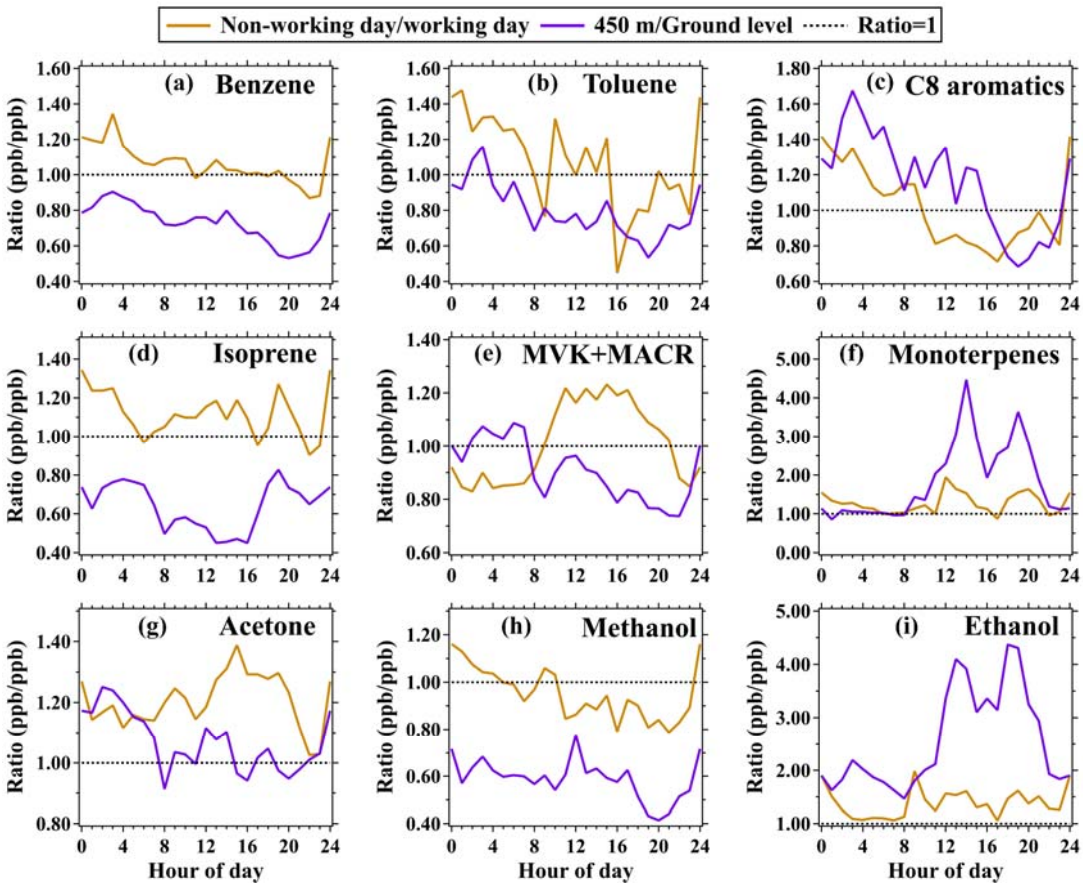

Figure S3. Diurnal variations in ratios of concentrations of the selected VOC species measured on non-working days to those measured on working days.

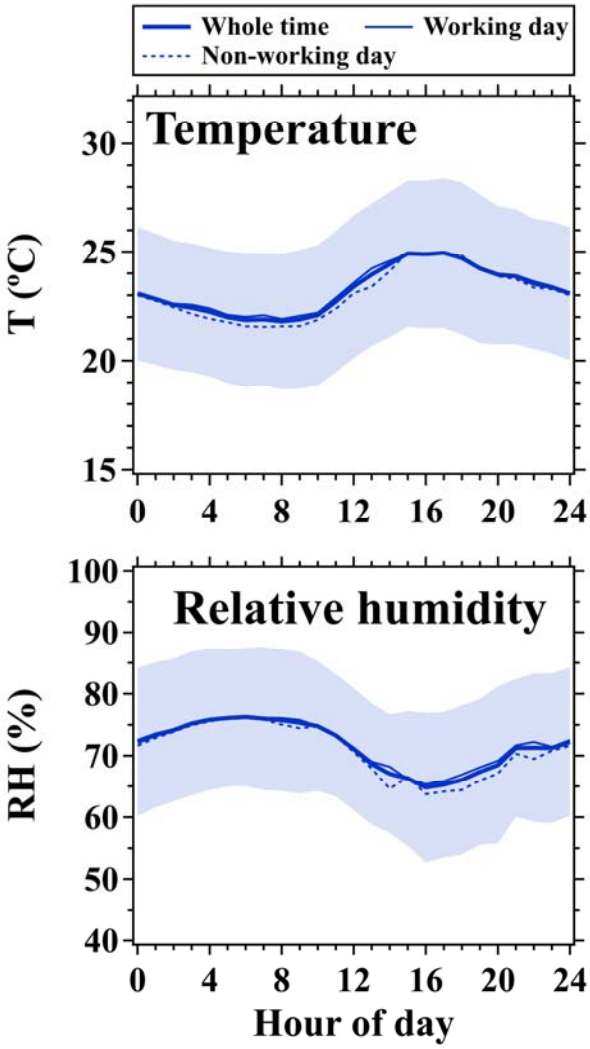

Figure S4. Diurnal variations in temperature (T) and relative humidity (RH) measured at 488 m. Thick blue solid lines and shaded areas represent averages and standard deviations during the CTT campaign; Thin blue solid and dashed lines represent averages on working and non-working days, respectively.

PMF receptor model

As expressed in Eq. (S1), the PMF model is a multivariate factor analysis tool that could decompose a data matrix $\boldsymbol{X}$ into two matrices including the source contribution matrix $\boldsymbol{g}$ and the source profile matrix $\boldsymbol{f}$ (Paatero and Tapper, 1994; Paatero et al., 2014).

$$X_{ij} = \sum_{k=1}^{p} g_{ik} \cdot f_{kj} + e_{ij} \tag{S1}$$

where i is the number of measured samples during the campaign, j is the number of measured chemical species, p is a user-defined number of sources, and $\boldsymbol{e}$ is the residual matrix. The PMF model is solved by minimizing the objective function Q using the measurement uncertainty matrix $\boldsymbol{U}$ and the residual matrix $\boldsymbol{e}$, as expressed in Eq. (S2),

$$Q = \sum_{i=1}^{n} \sum_{j=1}^{m} [\frac{e_{ij}}{U_{ij}}]^2 \tag{S2}$$

where n is the number of measured samples and j is the number of chemical species.

In this study, the 10-min mean mixing ratios of VOC species were used in the PMF model. The measurement uncertainty matrix $\boldsymbol{U}$ could be described in Eq. (S3),

$$U_{ij} = \sqrt{(NSR_{ij} \cdot x_{ij})^2 + (p_{1j} \cdot x_{ij})^2 + 2 \cdot \left(p_2 \cdot x_{ij}\right)^2 + LOD^2} \tag{S3}$$

where NSR_{ij} is the NSR for species j, as expressed in Eq. (S4); p_{1j} was assigned to 15% for the VOC species calibrated by the gas standard and LCU and 50% for the remaining VOC species; p_2 is the uncertainty caused by the utilization of mass flow controller (MFC) and was assigned to 1%. In this study, two MFCs were used in the calibration system: one for the gas standard and the other for the zero-air.

$$NSR_{ij} = \frac{\sqrt{C_{fj} \cdot x_{ij} \cdot t + 2 \cdot B \cdot t}}{C_{fj} \cdot x_{ij} \cdot t} \tag{S4}$$

where NSR_{ij} is the NSR for the ith sample of species j; C_{fj} and B are the average sensitivity and background signal of species j during the campaign; t is the time resolution (10 min) of VOC concentrations used in PMF.

In this study, a total of 225 chemical species (Table S1) were used in the PMF model to quantitatively analyze contributions of likely sources to the VOCs measurements made during the CTT campaign. VOC species with an SNR ≥ 1, 0.2 < SNR < 1, and SNR<0.2 were categorized as "strong", "weak", and "bad", respectively. The uncertainties of weak VOC species were doubled, while bad species were removed from the analysis. Figure S5 shows the change in $Q/Q_{expected}$ ratio with the increased number of factors in PMF. The $Q/Q_{expected}$ ratio decreased slowly when the number of factors increased from 5 to 6. In addition, profiles of two certain factors were highly correlated when the number of factors exceeded 5, resulting in an excessive decomposition of the VOCs measurements. As shown in Figure S6, the VOCs measurements were well reconstructed by a five-factor solution, which was deemed optimal for the PMF analysis in this study.

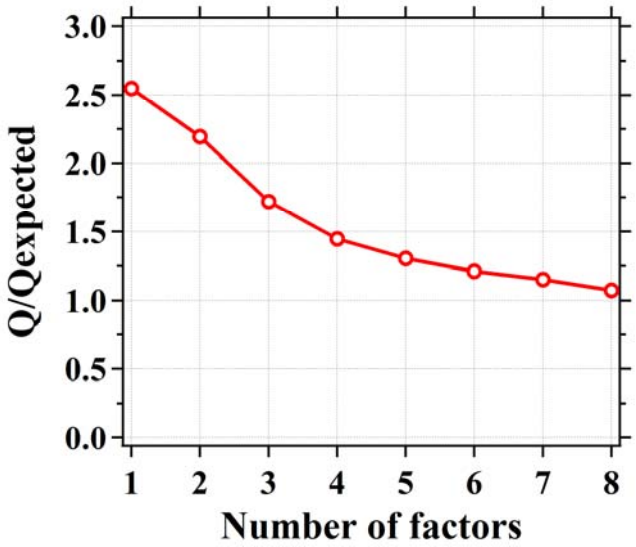

Figure S5. Variation in the ratio of $Q/Q_{expected}$ with change in the number of factors for the PMF analysis.

As shown in Figures 6 and S7, the most prominent composition in factor 1 were OVOC species including acetic acid, formaldehyde, acetone, methanol, acetaldehyde, hydroxyacetone, and formic acid, which contributed to over 70% of the concentration of the factor. These OVOC species with low molecular weights generally have complex sources in urban environments (Hu et al., 2013; Karl et al., 2018; McDonald et al., 2018; Pallavi et al., 2019; Gkatzelis et al., 2021), such as vehicular exhausts, various industrial

processes, biogenic emissions, as well as the oxidative degradation products of hydrocarbons. The diurnal profile of factor 1 increased between LT 09:00–14:00 and continuously decreased from LT 14:00 to 08:00 on the next day, which is consistent with the diurnal variation in ozone. Hourly mean contributions of factor 1 were also well correlated with those of ozone (r=0.75), implying strong dependence of factor 1 on sunlight and temperature. As a result, it is highly challenging to identify sources of factor 1 merely relying on its factor profile that does not contain dominant fingerprint species of specific emission sources. Therefore, factor 1 was assigned to the daytime-mixed source, predominantly including contributions from biogenic emissions, photooxidation products of various VOC species, and other emissions of sources that have strong dependences on solar radiation and temperature.

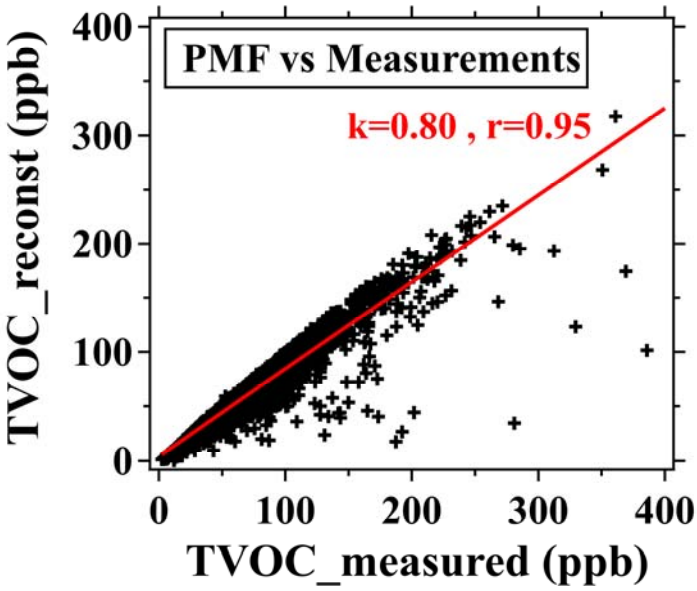

Figure S6. Scatter plots of PMF-reconstructed TVOC concentrations (TVOC_reconst) versus measured TVOC concentrations (TVOC_measured).

Factor 2 was characterized by a high percentage (72%) of ethanol and exhibited a similar diurnal pattern to ethanol. These results confirm that contributions of factor 2 were closely associated with visitor-related emissions. In addition, the contributions of factor 2 had the narrowest autocorrelation profile (Figure 6), implying that they were contributed by the most local emission sources. Thus, factor 2 was assigned to the visitor-related source, predominantly including contributions from human breath,

cooking, and the volatilization of ethanol-containing products and personal care products. It should be noted that large fractions of ethanol emitted from personal care products were generally attributed to the VCP source in previous studies (McDonald et al., 2018; Gkatzelis et al., 2021). This is correct when the observation site was not affected by intensive emissions from a known source such as visitors at the 450-m platform. The visitor-related source was resolved in PMF to separate contributions of VCPs from those emitted by visitors.

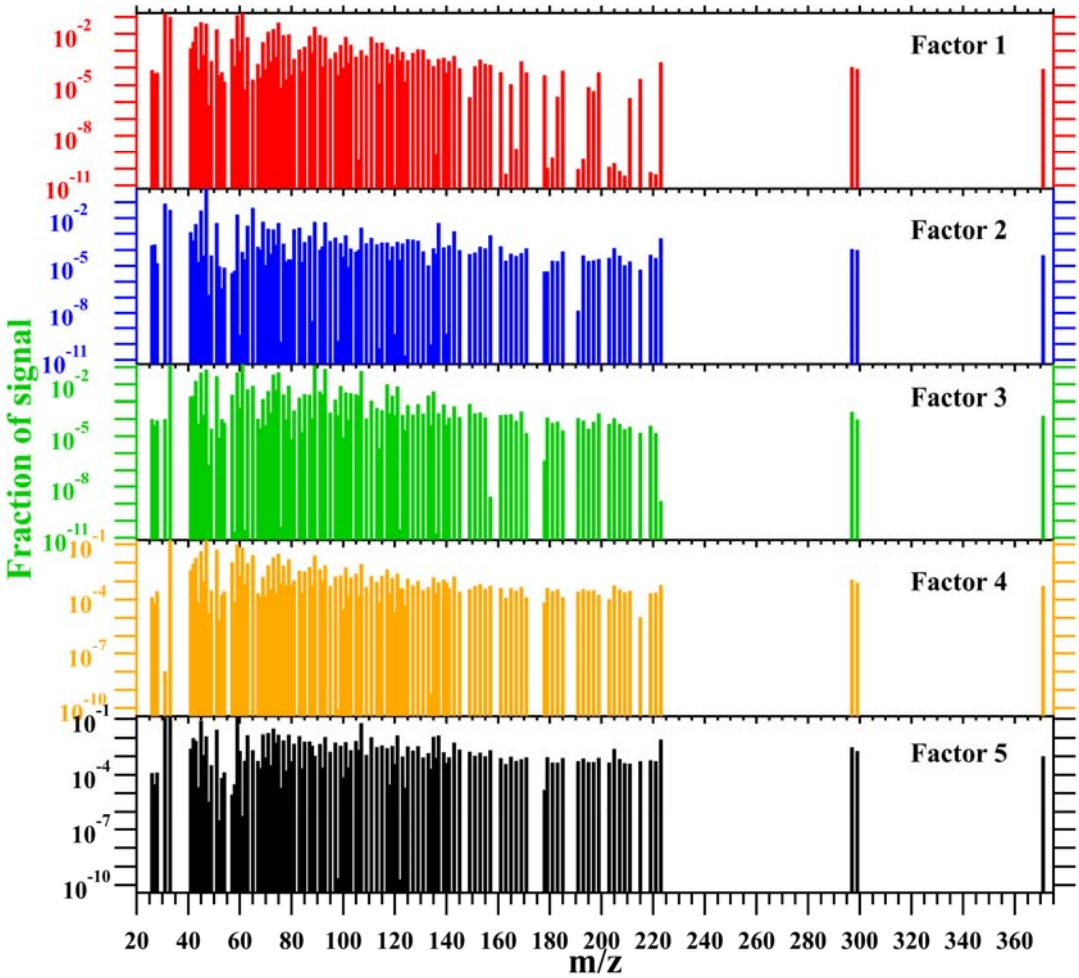

Figure S7. Factor profiles (covering the full range of the mass spectra) of the five factors resolved by the PMF model.

Factor 3 was primarily composed of acetic acid, methanol, ethyl acetate, toluene, ethanol, and C8 aromatics, contributing to over 62% of the concentration of the factor. The diurnal profile of factor 3 was highly consistent with those of aromatics, such as toluene, exhibiting lower mixing ratios during the daytime with a minimum occurring

at LT 14:00. Factor 3 explained over 90% and 70% of the variations in toluene and C8 aromatics, respectively, during the campaign. As reported in the literature (Zhang et al., 2013; Liu et al., 2016; Pallavi et al., 2019), aromatics are known components of vehicular exhausts, solvent usage, industrial raw materials, and emissions of various industrial processes. However, the PMF solution can not explicitly separate these sources in this study due to the lack of measurements for alkanes and low-carbon alkenes. In addition, factor 3 was less affected by visitor-related emissions due to its lower contributions during the opening hours of the 450-m platform on non-working days. Therefore, factor 3 was assigned to the vehicular+industrial source, predominantly including contributions from vehicular exhausts and emissions of various industrial processes.

Methanol, ethanol, acetone, and acetic acid were the most abundant species in factor 4, which contributed to over 51% of the concentration of the factor. The diurnal profile of factor 4 exhibited insignificant variability with slight increases between LT 08:00–13:00. Only a small fraction (<5%) of reactive chemical species such as aromatics were attributed to this factor. Factor 4 was also less affected by visitor-related emissions due to its lower contributions during the opening hours of the 450-m platform on non-working days. To further explore likely sources of factor 4, we also conducted a cluster analysis of 72-h backward trajectories, as detailed in the SI file. As shown in Figure S7, contributions of factor 4 accounted for 13% of the TVOC mixing ratio when affected by continental airflows, but only accounted for 3% when affected by marine airflows. However, contributions of the other factors displayed relatively weaker variations in different clusters of the backward trajectories. These results confirm that contributions of factor 4 had a strong dependence on wind direction and were highly associated with advection transport from nearby or distant cities. In addition, the contributions of factor 4 had the flattest autocorrelation profile (Figure 6), indicating that it was less affected by local emissions. Therefore, factor 4 was assigned to the regional transport source, predominantly including contributions from advection transport of aged air masses.

Methanol, acetone, formaldehyde, and acetaldehyde were the most prominent

species in factor 5, which contributed to over 46% of the concentration of the factor. In addition to contributions from secondary formation and vehicular exhausts, these OVOC species were also known components of VCPs (McDonald et al., 2018; Gkatzelis et al., 2021). As shown in Figure 6, the diurnal profile of factor 5 exhibited peak values between LT 08:00–09:00, during which personal care products were extensively used and vehicular exhausts were extensively emitted. Therefore, the diurnal variation pattern of factor 5 was similar to NOx (Figure 4), which is a typical tracer of vehicular exhausts in urban areas. The diurnal profile of factor 5 was also consistent with that of D5-siloxane, which is a key tracer for VCPs in urban environments (Tang et al., 2015; Gkatzelis et al., 2021). As shown in Figure 8, factor 5 contributed to a large fraction (45%) of D5-siloxane and had an ignorable contribution to toluene, confirming the predominant contributions of VCPs, rather than vehicular exhausts, in factor 5. Thus, factor 5 was assigned to the VCP-dominated source.

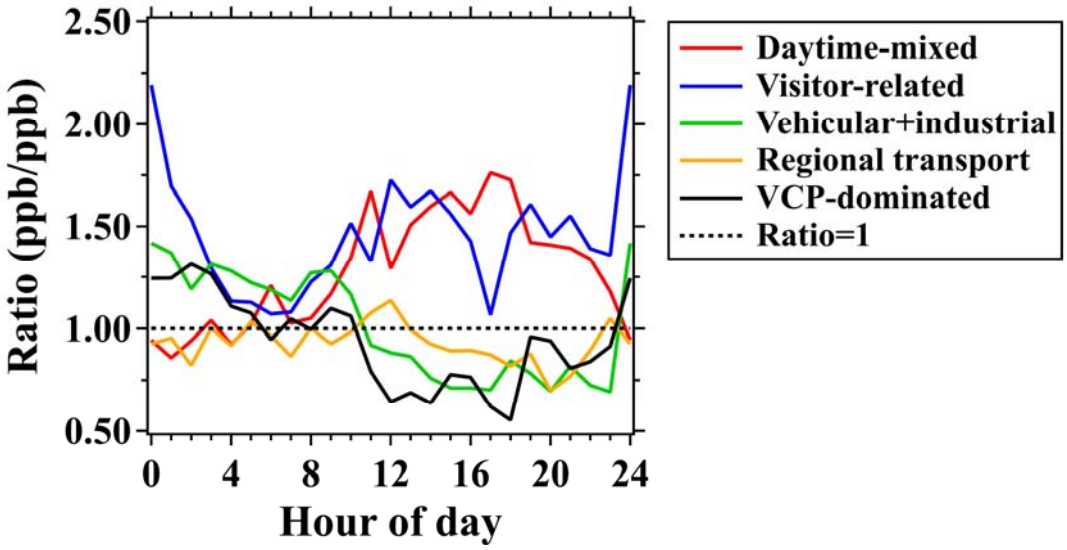

Figure S8. Average diurnal variations in ratios of contributions of the five PMF factors on non-working days to those on working days.

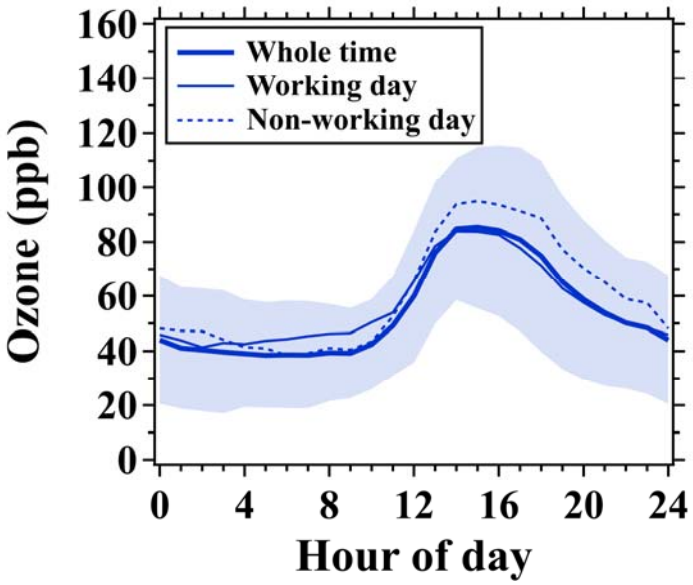

Figure S9. Diurnal variations in ozone mixing ratios measured at 488 m. Thick blue solid lines and shaded areas represent averages and standard deviations during the CTT campaign; Thin blue solid and dashed lines represent averages on working and non-working days, respectively.

Cluster analysis of backward trajectories

Backward trajectories (72 h) of air masses at an arrival altitude of 450 m over the CTT site were calculated for each hour during the campaign using the HYSPLIT Trajectory Model in MeteoInfo software (v 3.0.2). The backward trajectories were calculated based on meteorological data (one-degree resolution, global) from the GDAS system (ftp://ftp.arl.noaa.gov/pub/archives/gdas1) (Stein et al., 2015). Cluster analysis of the backward trajectories was performed in the MeteoInfo software using the K-means algorithm based on Euclidean distances (Wang, 2014), as shown in Figure S10.

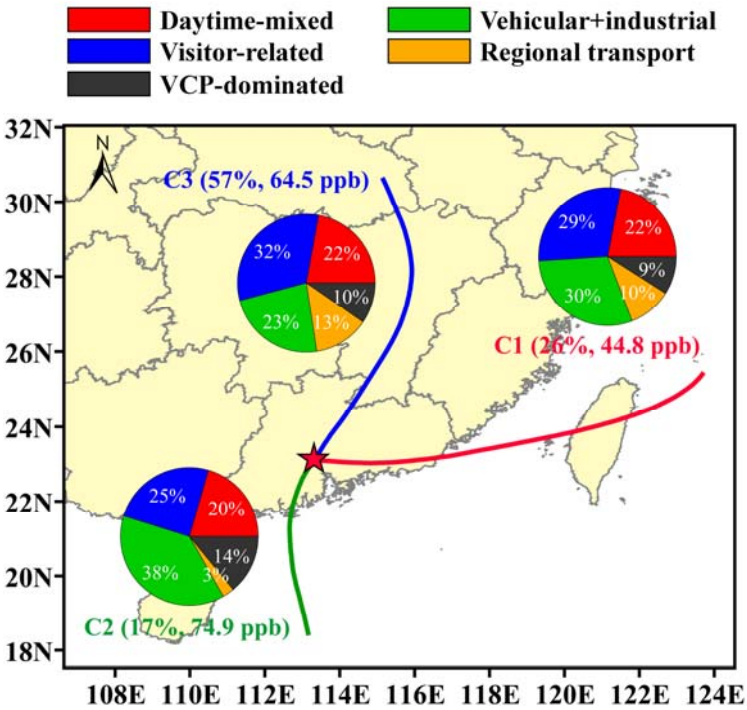

Figure S10. Cluster analysis of 72-h backward trajectories calculated for 24 hours on each day at an arrival altitude of 450 m above ground level at the CTT site. The red star indicates the CTT site. Pie charts indicate the average contributions of the five PMF factors in each cluster. The two digits in each parenthesis refer to the faction of the trajectories and the average TVOC concentration, respectively, in each cluster. C1, C2, and C3 indicate the three clusters of the trajectories, respectively.

Contributions of the five factors displayed strong variations during the campaign.

For example, contributions of the visitor-related and regional transport sources increased from October 3 to November 4, along with prominent decreases in contributions of the vehicular+industrial source. It indicates that the contributions of different sources had strong dependences on wind direction. As shown in Figure S10, the three clusters of air masses in this study are similar to those reported in the literature (Xia et al., 2021). Cluster 1, accounting for 26% of the backward trajectories, represents air masses that predominantly originated from the East China Sea and traveled over coastal regions before reaching the CTT site. Cluster 2, accounting for 17% of the backward trajectories, represents air masses that predominantly originated from the South China Sea and traveled over the southwest PRD region before reaching the CTT site. Cluster 3, accounting for 57% of the backward trajectories, represents air masses that predominantly originated from inland regions.

The average TVOC mixing ratios in the three clusters were 44.8, 74.9, and 64.5 ppb, respectively. Cluster 2 was characterized by the highest TVOC mixing ratios during the campaign with the largest contributions (38%) from the vehicular+industrial source. In addition, the regional transport source only contributed to 3% of TVOC mixing ratios in cluster 2 due to the marine origins of air masses. It implies that the measured TVOC mixing ratios were more contributed by local emissions with the higher fractions of reactive VOC species (such as aromatic species) when southwesterly winds prevailed over the PRD region, leading to a frequent occurrence of extremely high ozone mixing ratios. By contrast, contribution fractions of the vehicular+industrial source decreased to 30% and 23% in clusters 1 and 3, respectively, accompanied by significant increases in contributions of the regional transport source. Therefore, transport processes, driven by aged air masses from continental or coastal regions, were also important sources, contributing to over 10% of TVOCs mixing ratios. Contribution fractions of the daytime-mixed source slightly varied in the range of 20–22% among the three clusters of air masses, indicating a weaker wind direction dependence of the daytime-mixed source in comparison to other sources. The VCP-dominated source accounted for the highest fraction (14%) of TVOC mixing ratios in cluster 2 and comparable fractions in clusters 1 (9%) and 3 (10%), further confirming predominant

contributions of local anthropogenic emissions when affected by southeasterly air flows. The visitor-related source contributed to 32% and 29% of TVOC mixing ratios in clusters 1 and 3, respectively, which was greater than in cluster 1. The increased percentages of the visitor-related source in clusters 1 and 3 could be predominantly attributed to reduced contributions from the vehicular+industrial source. In addition, clusters 1 and 3 mainly occurred in the middle and late periods of the campaign, during which the 450-m platform took on more visitors with the successful control of the COVID-19 pandemic in China. Therefore, the larger numbers of visitors in clusters 1 and 3 were another important reason for the increased percentages of the visitor-related source in TVOC mixing ratios.

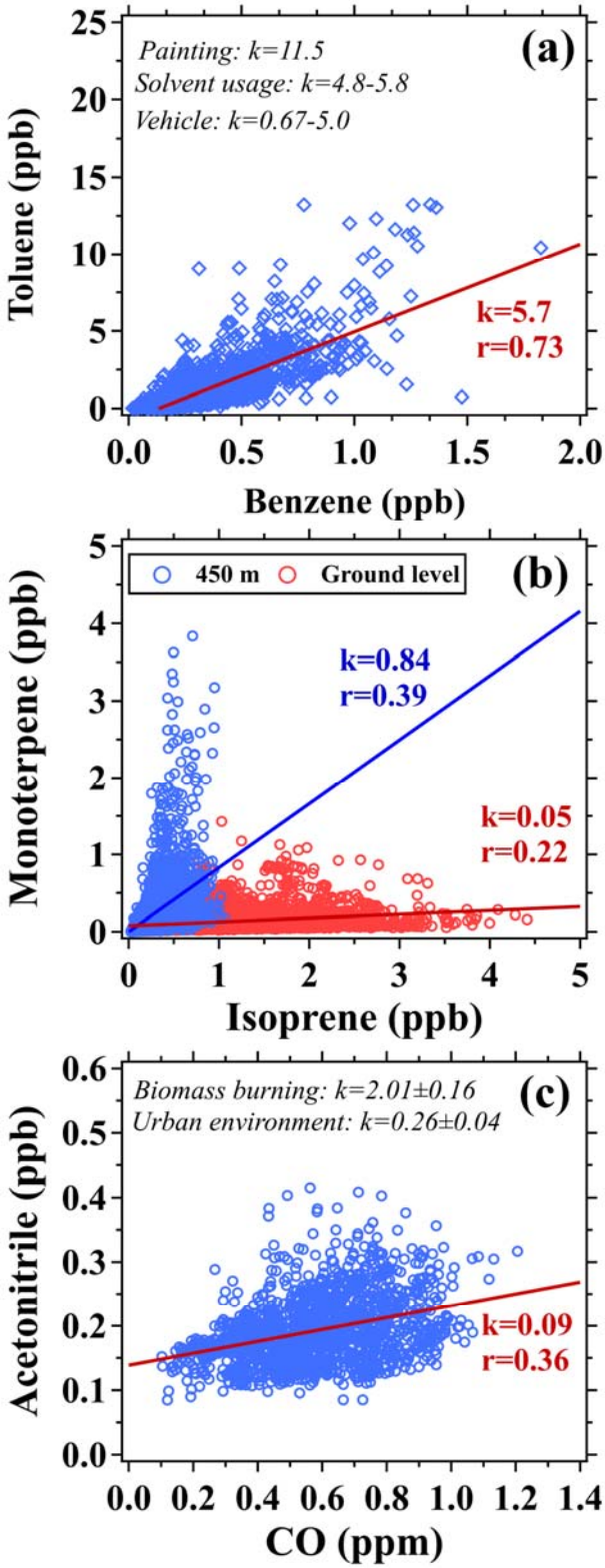

Figure S11. Scatter plots of (a) toluene versus benzene mixing ratios, (b) monoterpene versus isoprene mixing ratios in the daytime (LT 08:00–18:00), and (c) acetonitrile versus CO mixing ratios.

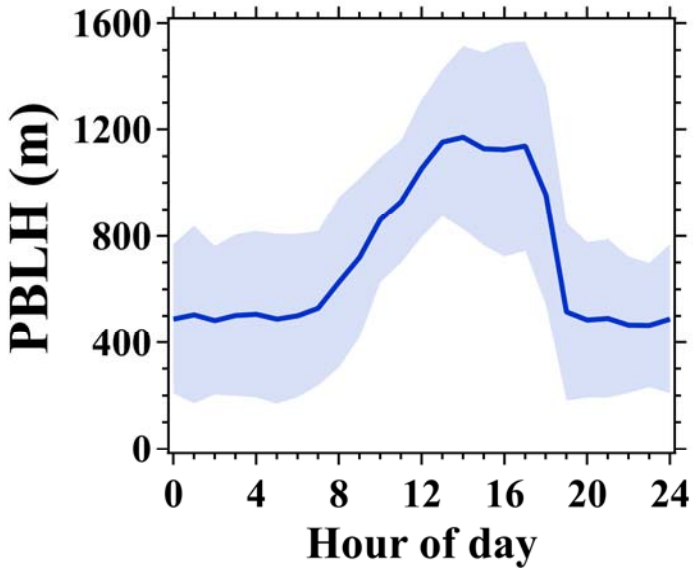

Figure S12. Diurnal variation in planetary boundary layer height (PBLH). Blue solid lines and shaded areas represent averages and standard deviations, respectively.

References

Gkatzelis, G. I., Coggon, M. M., McDonald, B. C., Peischl, J., Gilman, J. B., Aikin, K. C., Robinson, M. A., Canonaco, F., Prevot, A. S. H., Trainer, M., and Warneke, C.: Observations Confirm that Volatile Chemical Products Are a Major Source of Petrochemical Emissions in U.S. Cities, Environ Sci Technol, https://doi.org/10.1021/acs.est.0c05471, 2021.

Hu, L., Millet, D. B., Kim, S. Y., Wells, K. C., Griffis, T. J., Fischer, E. V., Helmig, D., Hueber, J., and Curtis, A. J.: North American acetone sources determined from tall tower measurements and inverse modeling, Atmos. Chem. Phys., 13, 3379-3392, https://doi.org/10.5194/acp-13-3379-2013, 2013.

Karl, T., Striednig, M., Graus, M., Hammerle, A., and Wohlfahrt, G.: Urban flux measurements reveal a large pool of oxygenated volatile organic compound emissions, Proceedings of the National Academy of Sciences of the United States of America, 115, 1186-1191, https://doi.org/10.1073/pnas.1714715115, 2018.

Liu, B., Liang, D., Yang, J., Dai, Q., Bi, X., Feng, Y., Yuan, J., Xiao, Z., Zhang, Y., and Xu, H.: Characterization and source apportionment of volatile organic compounds based on 1-year of observational data in Tianjin, China, Environ Pollut, 218, 757-769, https://doi.org/10.1016/j.envpol.2016.07.072, 2016.

McDonald, B. C., de Gouw, J. A., Gilman, J. B., Jathar, S. H., Akherati, A., Cappa, C. D., Jimenez, J. L., Lee-Taylor, J., Hayes, P. L., McKeen, S. A., Cui, Y. Y., Kim, S.-W., Gentner, D. R., Isaacman-VanWertz, G., Goldstein, A. H., Harley, R. A., Frost, G. J., Roberts, J. M., Ryerson, T. B., and Trainer, M.: Volatile chemical products emerging as largest petrochemical source of urban organic emissions, Science, 359, 760, https://doi.org/10.1126/science.aaq0524, 2018.

Paatero, P., and Tapper, U.: Positive matrix factorization: A non-negative factor model with optimal utilization of error estimates of data values, Environmetrics, 5, 111-126, https://doi.org/10.1002/env.3170050203, 1994.

Paatero, P., Eberly, S., Brown, S. G., and Norris, G. A.: Methods for estimating uncertainty in factor analytic solutions, Atmos. Meas. Tech., 7, 781-797, https://doi.org/10.5194/amt-7-781-2014, 2014.

Pallavi, Sinha, B., and Sinha, V.: Source apportionment of volatile organic compounds in the northwest Indo-Gangetic Plain using a positive matrix factorization model, Atmos. Chem. Phys., 19, 15467-15482, https://doi.org/10.5194/acp-19-15467-2019, 2019.

Stein, A. F., Draxler, R. R., Rolph, G. D., Stunder, B. J. B., Cohen, M. D., and Ngan, F.: NOAA'S HYSPLIT ATMOSPHERIC TRANSPORT AND DISPERSION MODELING SYSTEM, B Am Meteorol Soc, 96, 2059-2077, https://doi.org/10.1175/bams-d-14-00110.1, 2015.

Tang, X., Misztal, P. K., Nazaroff, W. W., and Goldstein, A. H.: Siloxanes Are the Most Abundant Volatile Organic Compound Emitted from Engineering Students in a Classroom, Environmental Science & Technology Letters, 2, 303-307, https://doi.org/10.1021/acs.estlett.5b00256, 2015.

Wang, Y. Q.: MeteoInfo: GIS software for meteorological data visualization and analysis, Meteorol Appl, 21, 360-368, https://doi.org/10.1002/met.1345, 2014.

Wu, C., Wang, C., Wang, S., Wang, W., Yuan, B., Qi, J., Wang, B., Wang, H., Wang, C., Song, W., Wang, X., Hu, W., Lou, S., Ye, C., Peng, Y., Wang, Z., Huangfu, Y., Xie, Y., Zhu, M., Zheng, J., Wang, X., Jiang, B., Zhang, Z., and Shao, M.: Measurement report: Important contributions of oxygenated compounds to emissions and chemistry of volatile organic compounds in urban air, Atmos. Chem. Phys., 20, 14769-14785, https://doi.org/10.5194/acp-20-14769-2020, 2020.

Xia, S.-Y., Wang, C., Zhu, B., Chen, X., Feng, N., Yu, G.-H., and Huang, X.-F.: Long-term observations of oxygenated volatile organic compounds (OVOCs) in an urban atmosphere in southern China, 2014–2019, Environ Pollut, 270, 116301, https://doi.org/10.1016/j.envpol.2020.116301, 2021.

Zhang, Y., Wang, X., Barletta, B., Simpson, I. J., Blake, D. R., Fu, X., Zhang, Z., He, Q., Liu, T., Zhao, X., and Ding, X.: Source attributions of hazardous aromatic hydrocarbons in urban, suburban and rural areas in the Pearl River Delta (PRD) region, J Hazard Mater, 250-251, 403-411, https://doi.org/10.1016/j.jhazmat.2013.02.023, 2013.